Performance evaluation and experimental study of a 0.34 THz folded waveguide sheet beam BWO

Jibran Latif

jlatif2012@gmail.com

University of Electronic Science and Technology of China

Huarong Gong

University of Electronic Science and Technology of China

Zhanliang Wang

University of Electronic Science and Technology of China

Atif Jameel

University of Electronic Science and Technology of China

Shaomeng Wang

University of Electronic Science and Technology of China

Jinjun Feng

Beijing Vaccum Electronic Research Institute

Yubin Gong

University of Electronic Science and Technology of China

Research Article

Keywords: Terahertz, backward wave oscillators, sheet beam, circular beam, interaction impedance, slow wave structure

Posted Date: September 12th, 2023

DOI: https://doi.org/10.21203/rs.3.rs-3326713/v1

Additional Declarations: No competing interests reported.

Version of Record: A version of this preprint was published at Journal of Infrared, Millimeter, and Terahertz Waves on March 25th, 2024. See the published version at https://doi.org/10.1007/s10762-024-

00980-3.

Noname manuscript No.
(will be inserted by the editor)

Performance evaluation and experimental study of a 0.34 THz folded waveguide sheet beam BWO

Jibran Latif · Huarong Gong · Zhanliang Wang · Atif Jameel · Shaomeng Wang · Jinjun Feng · Yubin Gong

Received: date / Accepted: date

Abstract Terahertz (THz) backward wave oscillators (BWOs) hold immense potential for a broad range of industrial and military applications. This study presents a comparative analysis of 0.34 THz sheet beam (SB) and circular beam (CB) folded waveguide (FWG) BWOs. We examined the design, simulation (CST MWS and PS, HFSS), and performance, revealing that sheet beam BWO outperforms circular beam BWO in terms of interaction impedance, power, efficiency, and bandwidth. Under 20 kV beam voltage and 10 mA beam current conditions, sheet beam BWO achieves 0.43 Ω (0.34 THz) interaction impedance, 1.3 W output power, and a bandwidth of approximately 12 GHz, surpassing the 0.16 Ω, 0.45 W and 8.5 GHz values of circular beam BWO, respectively. Furthermore, this study encompasses the fabrication and thorough characterization of the sheet beam BWO's slow wave structure. Experimental validation confirms its effectiveness, with measured S_{11} demonstrating reflection below -10 dB and S_{21} exhibiting transmission above -2 dB.

Keywords Terahertz · backward wave oscillators · sheet beam · circular beam · interaction impedance · slow wave structure

Jibran Latif · Atif Jameel
School of Electronic Science and Engineering, University of Electronic Science and Technology of China, Chengdu 610051, China. E-mail: jlatif2012@gmail.com; atif-jameel@std.uestc.edu.cn

Huarong Gong · Zhanliang Wang · Shaomeng Wang · Yubin Gong
National Key Laboratory of Science and Technology on Vacuum Electronics, University of Electronic Science and Technology of China, Chengdu, 610051, China. E-mail: hrgong@uestc.edu.cn; wangzl@uestc.edu.cn; wangsm@uestc.edu.cn; ybgong@uestc.edu.cn

Jinjun Feng
Beijing Vacuum Electronics Research Institute (BVERI), Beijing, China. E-mail: fengjj@ieee.org

1 Introduction and Background

Terahertz (THz) waves encompass electromagnetic frequencies ranging from 0.1 THz to 30 THz. Contemporary THz technology serves essential roles in advanced satellite communication systems designed for high-speed data transmission, medical imaging, non-destructive testing, plasma diagnostics, particle accelerators, environmental sensing, quality control in manufacturing, material characterization, etc [1]. The researchers have been putting enormous efforts into the development of efficient, compact, coherent, reliable, frequency agile, powerful, and cheaper THz devices [2]. BWOs are classical vacuum electron devices with the benefits of larger electronic tunability bandwidth, compact size, and better mechanical and thermal behavior. BWOs can produce higher continuous wave (CW) output powers in the THz band without requiring a pre-stage RF signal [3]. Folded waveguides (FWG) are promising slow-wave structures (SWS) used in BWOs for beam-wave interaction due to their compactness, higher power handling capability, enhanced interaction, and relatively easier manufacturing.

Almost all of the FWG SWS uses a circular channel for electron beams which has certain limitations. Devices employing sheet beams offer many advantages like high power density, enhanced beam spread control, reduced space charge effects, and better beam wave interaction. More output power from a device requires a high-power electron beam by either increasing the voltage or current. Electrical breakdown in the SWS may happen due to increased voltage of the beam beyond a certain level. Sheet beams handle this problem by spatially distributing the beam in one direction [1]. The sheet beam has been used in many THz vacuum electron devices but rarely in FWG SWS.

Researchers have presented various schemes of FWG BWOs, Travelling Wave Tubes (TWTs), and oscillators incorporating circular and sheet beams. In 2009, Rulin Zheng et al [4] studied parametric simulations and cold circuit properties of a 0.22 THz broadband circular beam FWG SWS for TWTs. M.H. Zhang et al [5] designed a 0.14 THz FWG sheet beam SWS for TWT with considerable bandwidth and 48% higher output power than conventional SWS in 2012. R. K. Sharma et al [6] analyzed FWG circular beam SWS for 0.1 THz TWT in 2014. Jinchi Cai et al [7] studied and presented a modified pillbox window as a power coupler part of FWG BWO at 0.22 THz. In 2016, Kunio Tsutaki et al [8] designed and fabricated a 0.3 THz FWG circular beam SWS for TWT amplifier using MEMS technology. Zhanliang Wang et al [9] designed and developed a 0.14 THz larger beam tunnel circular beam FWG SWS for TWT in 2017. Anurag Srivastava et al [10] studied the electrical design of a 0.22 THz circular beam FWG BWO and fabricated the SWS using multi-step photolithography and etching processes in 2019. Fengying Lu et al [1] presented a 0.22 THz sheet beam FWG oscillator and compared its performance with a circular beam oscillator.

In this article, a 0.34 THz folded waveguide sheet beam backward wave oscillator is designed, simulated, and fabricated using modern micro-fabrication techniques for cold test analysis. The design is compared in depth with a con-

ventional circular beam structure and it is found that the sheet beam FWG SWS shows better performance in terms of output power, frequency tunability, interaction impedance, bandwidth, and efficiency. As we know with the increasing frequencies in the THz region, the dimensions of the device become smaller. This makes the components of the device very hard to realize due to the mechanical limitations of the manufacturing techniques [11]. This research work is a successful effort to manufacture such small SWS with high precision and accuracy. The results of the simulation are experimentally validated in cold test analysis. A complete analytical and simulation model of the SWS is investigated in section 2. Particle-in-cell simulations are performed in section 3 for performance evaluation of both SB and CB BWO designs. Section 4 demonstrates the experimental validation of the proposed sheet beam BWO slow wave structure. Finally, the discussion, conclusion, and future works are provided in section 5.

2 Slow Wave Structure Design

The slow wave structure (SWS) is composed of a rectangular waveguide cleverly bent into a serpentine shape. This design serves the purpose of deliberately reducing the velocity of radio frequency (RF) power in precise coordination with the electron beam's movement. This synchronization maximizes the interaction between the electron beam and the RF signal while optimizing the transfer of power from the beam to the RF signal.

Within the SWS, a crucial alignment occurs, ensuring that the transverse component of the RF electric field aligns precisely with the direction of the electron beam at the interaction gaps. This alignment is pivotal for the effective functioning of the backward wave oscillator (BWO).

It's important to note that the BWO consistently operates in the backward wave mode. In this mode, the group velocity of the RF wave behaves inversely to the direction of the electron beam. This mode of operation is a fundamental characteristic of BWOs, enabling the generation of coherent electromagnetic radiation The SWS consists of a rectangular waveguide bent in the form of a serpentine. This design serves the purpose of slowing down the speed of RF power flow in precise coordination with the electron beam. This synchronism maximizes beam-wave interaction and power transfer from the beam to the RF signal. This SWS design also ensures that the transverse component of the RF E-field is aligned with the direction of the electron beam at the interaction gaps [12].

2.1 Analytical Design

Fig. 1 shows a unit cell of the FWG SWS in which p is the half period, s is the straight length of the waveguide, a and b are the length and width of the waveguide while a_1 and b_1 are the width and length of the beam tunnel

respectively. The parameter a of the waveguide decides the lower cutoff frequency f_c of the RF signal passing through the waveguide. The dimension b is chosen to ensure maximum on-axis E-Field and interaction impedance. The fundamental TE_{10} mode is assumed to be propagating along the waveguide. Because of the periodic design of the structure, numerous spatial harmonics become enabled. The phase shift of the mth spatial harmonics is given by [1];

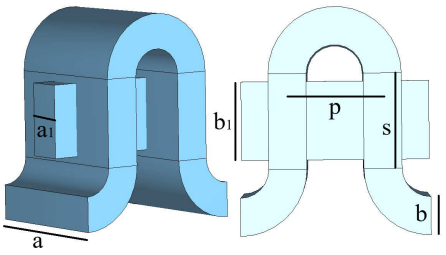

Fig. 1: The vacuum model of a unit cell of the FWG SWS

$$\phi = \beta_m p = (s + \frac{\pi}{2} p)\beta_{wg} + (2m + 1)\pi \tag{1}$$

where β_{wg} is the propagation constant and m is the spatial harmonics order. The electron beam interacts with the fundamental spatial harmonic of the backward wave RF field with a phase shift of $\beta_m p = \frac{5\pi}{2}$ radians. The beam voltage is chosen to be 20 kV and the beam current to be 10 mA (must be greater than the minimum starting oscillation current). The beam velocity is related to the voltage as [10];

$$v_b = \sqrt{\frac{2eV}{m}} \tag{2}$$

where V is the applied voltage in volts, e is the charge on an electron in coulombs and m is the mass of an electron in kilograms. The value of the beam velocity is approximately $0.28c$ (c=speed of light). We estimate the value of "p" by aligning the beam velocity with the velocity of the SWS. The phase velocity can be determined using the following relationships [13]:

$$v_p = \frac{2\pi f}{\frac{\phi}{2}} \tag{3}$$

$$\frac{v_p}{c} = [\frac{s + \frac{\pi}{2} p}{p} \sqrt{1 - (\frac{\omega_c}{\omega})^2} + \frac{(2m + 1)\pi}{p}]^{-1} \tag{4}$$

2.2 High-Frequency Characteristics

The cutoff angular frequency of a rectangular waveguide with TE_{10} fundamental propagating mode is $\omega_c = \frac{\pi c}{a}$. Therefore the dispersion can be expressed as [12]:

$$\omega^2 = \omega_c^2 + k^2 c^2 \tag{5}$$

where ω represents the angular frequency measured in radians, and k stands for the wave number along the axis of the curved waveguide. From the standpoint of beam-wave interaction, the beam observes the phaseshift from one gap to the next as given below [1]:

$$\phi_z = k(s + \frac{p}{2}\pi) + \pi \tag{6}$$

The second term of the above equation represents an extra phase shift of π due to the bending of the waveguide introducing a reversal of the direction of the E-field as seen along the direction of propagation of the beam. Equations 5 and 6 together give us the dispersion relations for the folded waveguide and can be conveniently expressed in a simplified form as [10]:

$$f = f_c \sqrt{1 + (\frac{a}{s + \frac{p}{2}\pi})^2 [\frac{\phi_z}{\pi} - (2m+1)]^2} \tag{7}$$

The integer $m(0, 1, 2, 3, \ldots\ldots)$ represents the order of the spatial harmonics due to the repetitive nature of the structure. The beam modulation frequency at different voltages is $f_m = \frac{v_z \phi_z}{2p\pi}$ (v_z is the axial velocity of the wave). Based on the above-mentioned analytical relations and using the high-frequency solver of the CST MWS, the beam-wave dispersion plot of the structure is plotted as shown in Fig. 2.

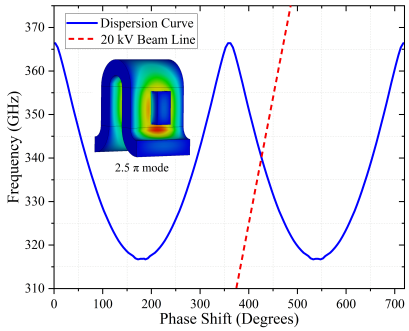

Fig. 2: Dispersion characteristics of the FWG SWS showing the operating point at a beam voltage of 20 kV

It can be seen that the 20 kV beam line intersects with the dispersion curve at a phase shift of 2.5 π radians. The structure is optimized to have the

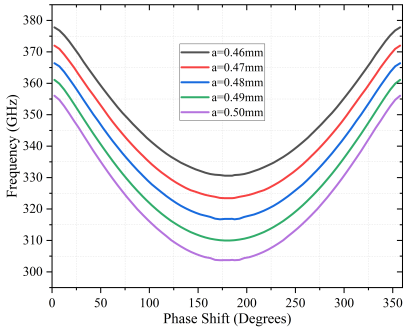

(a) Effect of a on dispersion characteristics

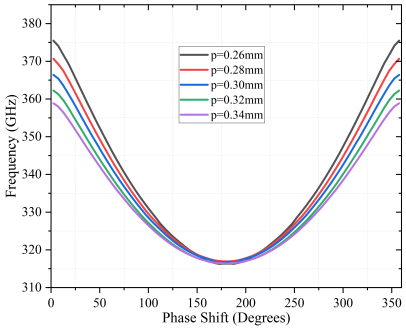

(b) Effect of p on dispersion characteristics

Fig. 3: Effect of various geometrical parameters of SWS on the dispersion characteristics

intersection point close to the center of the lower and higher frequency limits of the dominant mode to ensure maximum bandwidth and voltage tunability while keeping the device in the backward region of operation. It is worth mentioning here that to operate the device in $\pi/2$ mode, we have to increase the voltage beyond 1000 kV which is not possible due to the miniaturized nature of the structure.

To obtain the most suitable geometric parameters for the slow wave structure, the effect of each of these parameters is analyzed using CST MWS and HFSS. The effect of changing a and p on the dispersion characteristic curve of the SWS is shown in Fig. 3. It can be seen from Fig. 3 that as the broader width of the waveguide drops from a=0.50 mm to a=0.46 mm, the passband gap of the SWS increases from 0.303-0.355 THz to 0.330-0.377 THz. The waveguide width a is thus a key parameter in determining the dispersion of the structure. The other parameters b, s and p mainly affect the upper frequencies of the dispersion curve.

2.3 Interaction Impedance

The amount of E-field on an axis that is available for a given propagating power in the waveguide is numerically represented by interaction impedance. This factor is greatly affected by the dimensions of the beam tunnel. If the beam tunnel is small, a large magnetic focusing field will be required and transportation of the beam through the tunnel without interception with the walls of the tunnel will be difficult. Electron debunching takes place, significantly diminishing the structure's amplification potential because of heightened space-charge effects. Furthermore, if the tunnel dimensions are excessively spacious, there's a risk of RF power leaking from the waveguide into the tunnel. This leakage results in a reduction of the net E-field accessible for beam-wave interaction, consequently lowering the gain [14]. Therefore, the optimum dimensions of the

beam tunnel need to be found based on the analytical analysis of interaction impedance.

Assume that an electron beam is propagating along the z-axis in the SWS. The interaction impedance can be written as [15,16];

$$K_c = \frac{|E_n|^2}{2\beta^2 P_f} \tag{8}$$

where E_n is the E-field of the nth space harmonic and, P_f is the power flow through the structure which can be calculated from group velocity and stored energy

$$P_f = \frac{v_g W}{2p} \tag{9}$$

The on-axis E-field E_z of the mth space harmonic is expressed mathematically as [15];

$$E_z(z) = \sum_{m=-\infty}^{\infty} E_n e^{-jk_n z} \tag{10}$$

$$E_n = \frac{1}{2p} \int_0^{2p} E_z(z) e^{jk_n z} dz \tag{11}$$

The interaction impedance is greatly influenced by the geometry of the beam tunnel as well as the distribution of the E-field and H-field around the tunnel. The interaction impedance for both the sheet beam FWG SWS and circular beam FWG SWS were calculated at the point of beam-wave interaction in the beam tunnel and are shown in Fig. 4. The High-Frequency Structure Simulator (HFSS) software is used for this purpose.

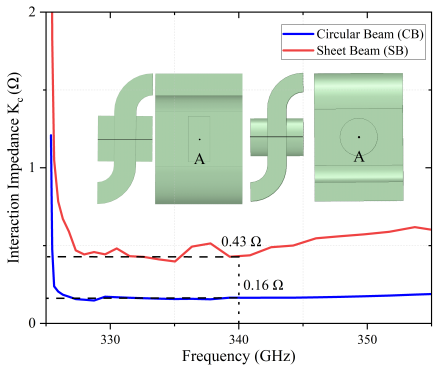

Fig. 4: On-axis interaction impedance for the SB FWG SWS and the CB FWG SWS.

It can be seen that the interaction impedance is far greater in the sheet beam FWG SWS as compared to the circular beam FWG SWS having the

same dimensions as the SB structure (except for the beam tunnel). The overall cross-sectional area of the beam tunnels for both structures is kept the same. The extended shape of the SB tunnel in one direction ensures better confinement of the field within the waveguide which leads to better interaction between the beam and the electromagnetic waves. The value of the interaction impedance for the SB and the CB at 0.34 THz is around 0.43 Ω and 0.16 Ω respectively.

Based on the above analytical analysis, for a 0.34 THz BWO, a well-optimized set of parameters is calculated using the CST MWS, PS and HFSS. Table 1 shows the optimized values of the design parameters of the structure.

Table 1: Optimized values of design parameters for the 0.34 THz FWG SWS of the BWO

a	b	s	p	a_1	b_1
0.48 mm	0.12 mm	0.30 mm	0.30 mm	0.16 mm	0.25 mm

3 Particle-in-Cell (PIC) Simulations

In order to anticipate the performance of the engineered slow wave structure, we executed a 3D Particle-in-Cell (PIC) simulation. The CST Studio software served as the tool for evaluating various aspects, including beam-wave interaction, output power, resonant frequency, tunability, bandwidth, and efficiency The size of the SWS in Terahertz devices is extremely small and the fabrication process may introduce uncertainties in device performance characteristics. Although modern fabrication techniques are quite precise, the skin depth and surface roughness may become comparable in dimension. To account for these two factors, annealed copper with a conductivity of 4.3×10^7 S/m and surface roughness of approximately 100 nm is used in PIC simulations [1]. To compare the performance of circular beam SWS and sheet beam SWS for BWO, 3D models of both designs are constructed. The only difference is the beam tunnel in both designs. To achieve the best possible estimation of the performance comparison, the areas of the beam tunnels in both cases are kept the same. All other parameters like beam voltage, current, rise time, number of periods, and SWS dimensions are also kept the same for both cases. A constant magnetic field of 0.3 T is applied along the axial direction for beam focusing. Fig. 5 shows the complete PIC simulation model of the SWS for the SB FWG BWO. It is comprised of 90 periods. The top and side views of the beam trajectory clearly show the bunching of electrons in the tunnel due to sudden acceleration and deceleration. The front view shows the rectangular beam particle trajectory of the sheet beam. Couplers were also designed to extract the RF power from the SWS and to later connect the SWS to the Vector Network Analyzer (VNA) for cold test analysis.

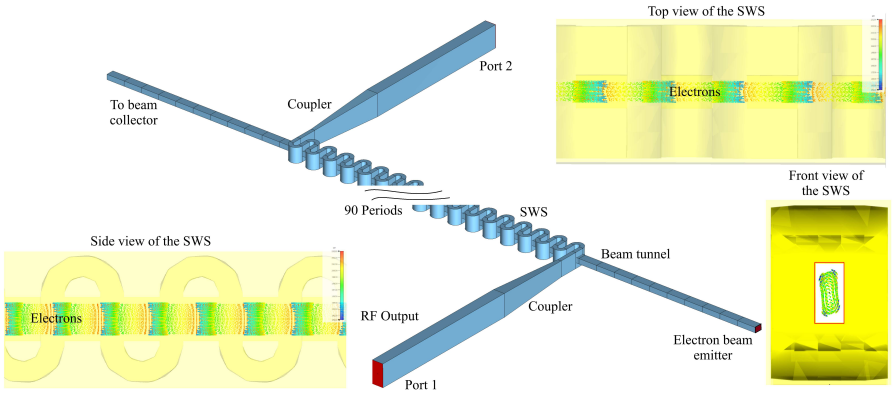

Fig. 5: Complete PIC simulation model of the SB FWG SWS along with couplers

3.1 Coupler Design

Fig. 6 shows the transmission and reflection characteristics of the couplers along with the E-field contour plots. The field plots indicate the propagation of dominant TE_{10} mode on both sides of the coupler. Port 1 of the couplers is connected to the SWS while Port 2 is connected to the standard WR2.8 (260-400 GHz) waveguide flange for connection with the VNA. The S_{11} is approximately -33 dB and S_{21} is almost 0 dB. These values clearly indicate negligible reflection and good transmission of the RF power.

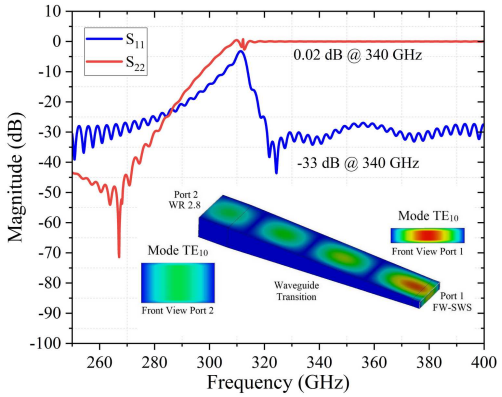

Fig. 6: Transmission and reflection characteristics of the couplers with field plots

3.2 Output Power and Frequency

The output port signals of both the SB and CB designs are shown in Fig. 7a for the same beam voltage of 20 kV and beam current of 10 mA. A stable and saturated output power of approximately 1.3 W (square of the output port signal) is obtained by the sheet beam BWO which is much higher than the 0.45 W as obtained by CB BWO. Also, the oscillations start a little bit earlier in the SB SWS due to the larger contact area of the beam and the waves. Fig. 7b shows the frequency spectrums for both SB and CB BWOs. The RF port signal in SB oscillates at approximately 0.34 THz while the CB BWO shows oscillations at approximately 0.343 THz. This small difference is due to the change in beam tunnel geometry.

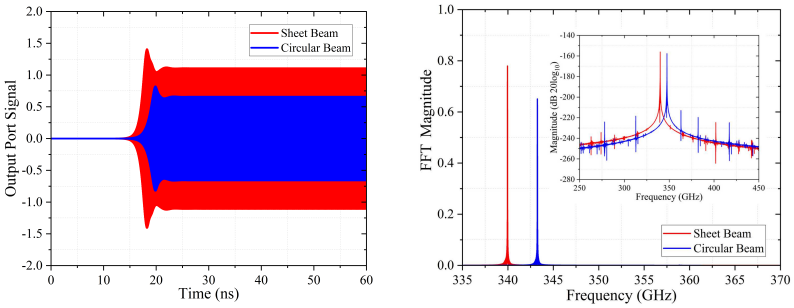

(a) Output port signal vs time (b) Frequency spectrum characteristics

Fig. 7: Comparison of output power and FFTs of SB and CB BWOs

3.3 Tunability and Bandwidth

To further study the effects of external variables like beam voltage, various simulations were performed under changing beam voltage for both SB and CB BWOs. The electronic tunability capability of the proposed SB BWO along with CB BWO is shown in Fig. 8a. It can be seen that for the SB BWO, the frequency changes linearly with a slope of approximately 2 GHz/kV, and for the CB BWO, the slope is approximately 1.25 GHz/kV. When the beam voltage changes from 16 kV to 25 kV, the oscillation frequency changes from 0.33 THz to 0.35 THz for the SB BWO and the frequency changes from 0.335 THz to 0.347 THz for the CB BWO. The performance of the SB BWO remains acceptable in this operating region with a peak output power of 1.3 W at 0.34 THz and 20 kV. Fig. 8b shows the power vs. frequency characteristics of both devices from which -3 dB bandwidth can be easily calculated. The bandwidth of the designed SB BWO is approximately 12 GHz while the CB BWO offers a bandwidth of approximately 8.5 GHz. This is because the wider

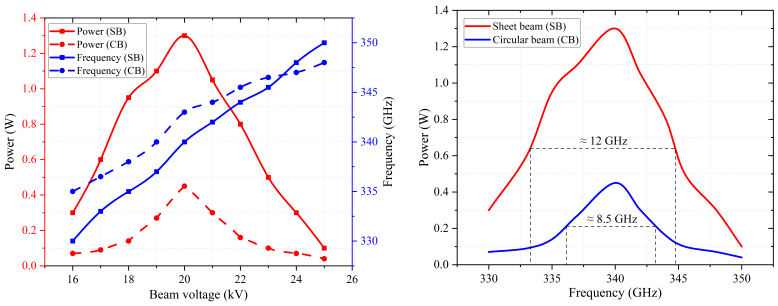

(a) Peak output power and frequency vs beam voltage

(b) Power vs frequency showing -3 dB bandwidth

Fig. 8: Electrical tunability characteristics and -3 dB bandwidth of both BWOs

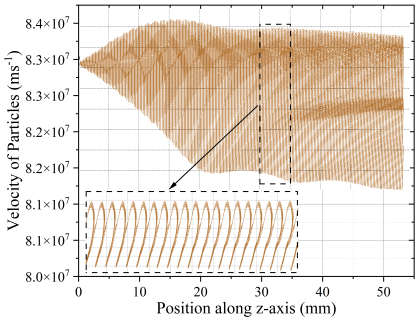

Fig. 9: Velocity of beam particles as they move along the beam tunnel

beam profile of the sheet beam enables it to engage with a more extensive spectrum of electromagnetic modes within the slow wave structure, resulting in an increased bandwidth. Thus, the sheet beam BWO clearly has advantages over circular beam BWO in terms of output power, tunability, and bandwidth.

3.4 Beam-Wave Power Transfer

Phase space analysis of the complete structure is performed to observe the transfer of power from the electron beam into the electromagnetic waves. Fig. 9 shows the velocity of particles of the beam as they move along the tunnel. It can be seen that the overall velocity of particles tends to decrease along the tunnel due to the loss of energy. The power is continuously transferred from the beam to the generated electromagnetic waves.

4 Cold Test Analysis

The main task in the fabrication of a SWS at such high frequency is the realization of the surface roughness of the waveguide lower than the skin depth (0.112 μm at 0.34 THz for Cu material). Reduced surface roughness ensures fewer ohmic losses in the structure during operation. The alignment of the structure within a tolerance of approximately 5-10 μm is also considered important. To verify the design, the SWS has been fabricated using oxygen-free copper (OFC). Fig. 10 shows the complete 3D geometry of the manufactured SWS in Siemens NX 12.0. The SWS has been manufactured in 2 halves which are

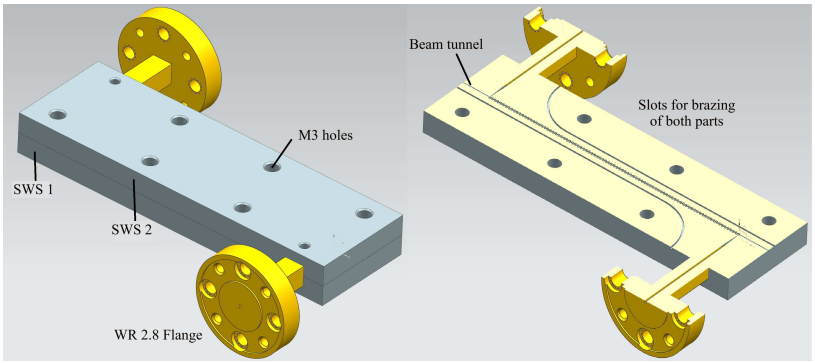

Fig. 10: 3D model of the SWS

braze-welded together. The two flanges are designed to match with a standard WR 2.8 rectangular waveguide. The overall length of the SWS is approximately 65mm. The transmission (S_{21}) and reflection characteristics (S_{11}) of the manufactured SWS were measured by the Ceyear 3672D Vector Network Analyzer (VNA) and the Ceyear 3643TA VNA extender. Fig. 11 shows the manufactured parts of the SWS along with the experimental setup. The microscopic zoomed-in view of the folded SWS shows a clear and smooth surface of the structure.

Fig. 12 shows the simulated and measured S-parameters of the SWS. It can be seen that the experimental results are well in accordance with the simulations. The slight differences can be due to limitations in machining accuracies, assembly, and alignment tolerance of two halves and calibration errors during actual measurements on VNA. The measured S_{21} is higher than -2 dB over a frequency range of 0.335 - 0.345 THz and S_{11} is lower than -10 dB over the same frequency range.

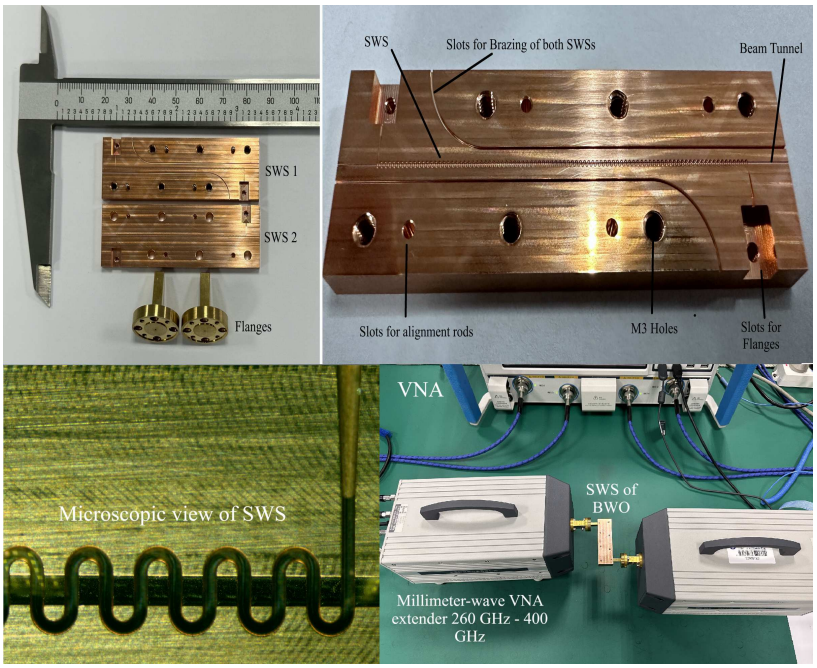

Fig. 11: Manufactured SWS along with experimental setup

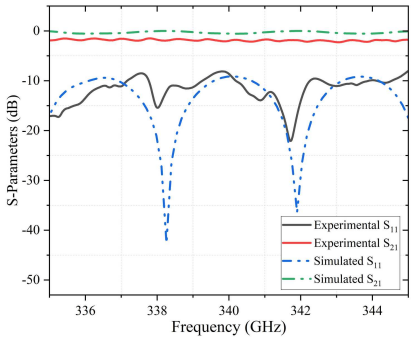

Fig. 12: Comparison of the simulated and measured transmission and reflection characteristics of the SWS

5 Conclusion

In this study, we conducted a comprehensive investigation into the design, simulation, and performance evaluation of sheet beam and circular beam folded waveguide backward wave oscillators (BWOs) operating at 0.34 THz.Our findings illuminated the considerable potential of sheet beam BWOs in the terahertz regime. Under identical conditions of 20 kV beam voltage and 10 mA

beam current, the sheet beam BWO consistently outperformed its circular beam counterpart. It exhibited superior interaction impedance, power output, and bandwidth. With an output power of 1.3 W, an interaction impedance of 0.43 Ω, and a broad bandwidth of approximately 12 GHz, the sheet beam BWO showcased its capability to meet the demands of the terahertz applications. Additionally, our work encompassed the manufacturing and meticulous characterization of the sheet beam BWO's slow wave structure. Through experimental validation, we confirmed the efficacy of this critical component at 0.34 THz frequency. The measured S_{11} demonstrated significant reflection, surpassing -10 dB, while S_{21} exhibited transmission above -2 dB. We are planning to design the electron optical system and electron gun for this SWS in the future for a hot test. In sum, the observed advantages of sheet beam BWOs in terms of power, interaction impedance, and bandwidth open new avenues for advancing terahertz technology, offering enhanced capabilities for applications ranging from advanced imaging to communication systems. This work serves as a stepping stone for future research and development in this promising field, enabling the harnessing of terahertz frequencies for an array of military, industrial, and scientific endeavors.

Acknowledgements

This work is supported by the National Natural Science Foundation of China under (Grant Nos. 61531010, 61371052, and 61871095) and by the Key R&D Program of Guangdong (Grant No. 2021B0101300003) and the National Key Research and Development Program of China (Grant No. G072022YFF0707602).

Declarations

Ethical Approval: Not applicable.
Competing Interests: We declare that there are no competing interests, financial or personal, associated with this manuscript.
Authors' Contributions: All of the authors made significant contributions to this research. Mr. Jibran, Mr. Huarong, Mr. Zhanliang worked on the design, simulation, fabrication, and writing process. Mr. Jinjun worked on the validation of simulation results. Mr. Shaomeng and Mr. Yubin worked on reviewing the manuscript. Mr. Atif worked on all the figures.
Funding: This work is supported by the National Natural Science Foundation of China under (Grant Nos. 61531010, 61371052, and 61871095) and by the Key R&D Program of Guangdong (Grant No. 2021B0101300003) and the National Key Research and Development Program of China (Grant No. G072022YFF0707602).
Availability of Data and Materials: Any interested person or party can access the relevant data of this research by contacting Mr. Jibran via his email.

References

1. Fengying Lu, Ke Li, Zhixiong Lei, Ming Huang, and Wensheng Qiao. Study of a terahertz folded waveguide oscillator with sheet electron beam. *AIP Advances*, 11(4):045012, 2021.
2. Ruifeng Zhang, Qi Wang, Difu Deng, Yao Dong, Fei Xiao, Gil Travish, and Huarong Gong. Novel dual beam cascaded schemes for 346 ghz harmonic-enhanced twts. *Electronics*, 10(2):195, 2021.
3. Yan Na Tang, Li Shi, Wen Qiu Xie, and Zi Cheng Wang. Research on the 650ghz folded waveguide bwo. In *Applied Mechanics and Materials*, volume 644, pages 4099–4102. Trans Tech Publ, 2014.
4. Ruilin Zheng and Xuyuan Chen. Parametric simulation and optimization of cold-test properties for a 220 ghz broadband folded waveguide traveling-wave tube. *Journal of Infrared, Millimeter, and Terahertz Waves*, 30:945–958, 2009.
5. MH Zhang, YY Wei, G Guo, LN Yue, Y Hou, SM Wang, J Xu, YB Gong, and WX Wang. A novel 140-ghz sheet-beam folded-waveguide traveling-wave tube. *Journal of Electromagnetic Waves and Applications*, 26(17-18):2332–2340, 2012.
6. Rajendra Kumar Sharma, Andre Grede, Shailendra Chaudhary, Vishnu Srivastava, and Heino Henke. Design of folded waveguide slow-wave structure for w-band twt. *IEEE Transactions on Plasma Science*, 42(10):3430–3436, 2014.
7. Jinchi Cai, Linlin Hu, Guowu Ma, Hongbin Chen, Xiao Jin, and Huanbi Chen. Theoretical and experimental study of the modified pill-box window for the 220-ghz folded waveguide bwo. *IEEE Transactions on Plasma Science*, 42(10):3349–3357, 2014.
8. Kunio Tsutaki, Yoichiro Neo, Hidenori Mimura, Norio Masuda, and Mitsuru Yoshida. Design of a 300 ghz band twt with a folded waveguide fabricated by microelectromechanical systems. *Journal of Infrared, Millimeter, and Terahertz Waves*, 37:1166–1172, 2016.
9. Zhanliang Wang, Qing Zhou, Huarong Gong, Junpeng Liao, Yanyu Wei, Zhaoyun Duan, Hongwei Liu, and Yubin Gong. Development of a 140-ghz folded-waveguide traveling-wave tube in a relatively larger circular electron beam tunnel. *Journal of ElEctromagnEtic WavEs and applications*, 31(17):1914–1923, 2017.
10. Anurag Srivastava, Siva Penmetsa, Latha Christie, and KN Bhat. Electromagnetic design of a 220 ghz bwo with experimental study of micro-fabricated folded waveguide structure. *Journal of Electromagnetic Waves and Applications*, 33(14):1860–1873, 2019.
11. Rakesh Kumar Bhardwaj, HS Sudhamani, VP Dutta, and Naresh Bhatnagar. Micromachining and characterisation of folded waveguide structure at 0.22 thz. *Journal of Infrared, Millimeter, and Terahertz Waves*, 42:229–238, 2021.
12. Khanh T Nguyen, Alexander N Vlasov, Lars Ludeking, Colin D Joye, Alan M Cook, Jeffrey P Calame, John A Pasour, Dean E Pershing, Edward L Wright, Simon J Cooke, et al. Design methodology and experimental verification of serpentine/folded-waveguide twts. *IEEE Transactions on Electron Devices*, 61(6):1679–1686, 2014.
13. Changqing Zhang and Yubin Gong. Analytical exploration of folded waveguide circuit design for high-power traveling-wave tube amplifier. *Journal of Infrared, Millimeter, and Terahertz Waves*, 32:407–417, 2011.
14. RA Stuart, CC Wright, AI Al-Shamma'a, J Lucas, and YS Tan. The dimensions of the electron beam tunnel in a folded waveguide twt. In *2005 Joint 30th International Conference on Infrared and Millimeter Waves and 13th International Conference on Terahertz Electronics*, volume 2, pages 545–546. IEEE, 2005.
15. John H Booske, Mark C Converse, Carol L Kory, Christine T Chevalier, David A Gallagher, Kenneth E Kreischer, Vernon O Heinen, and Sudeep Bhattacharjee. Accurate parametric modeling of folded waveguide circuits for millimeter-wave traveling wave tubes. *IEEE Transactions on Electron Devices*, 52(5):685–694, 2005.
16. BN Basu. *Electromagnetic theory and applications in beam-wave electronics*. World scientific, 1996.